Mapping Exoplanets

Nicolas B. Cowan and Yuka Fujii

Contents

Abstract

The varied surfaces and atmospheres of planets make them interesting places to live, explore, and study from afar. Unfortunately, the great distance to even the closest exoplanets makes it impossible to resolve their disk with current or near-term technology. It is still possible, however, to deduce spatial inhomogeneities in exoplanets provided that different regions are visible at different times – this can be due to rotation, orbital motion, and occultations by a star, planet, or moon. Astronomers have so far constructed maps of thermal emission and albedo for short-period giant planets. These maps constrain atmospheric dynamics and cloud patterns in exotic atmospheres. In the future, exo-cartography could yield surface maps of terrestrial planets, hinting at the geophysical and geochemical processes that shape them.

N.B. Cowan (✉)
McGill University, Montréal, QC, Canada
e-mail: nicolas.cowan@mcgill.ca

Y. Fujii
Earth-Life Science Institute, Tokyo Institute of Technology, Tokyo, Japan
e-mail: yuka.fujii.ebihara@gmail.com

H.J. Deeg, J.A. Belmonte (eds.), *Handbook of Exoplanets*,
https://doi.org/10.1007/978-3-319-30648-3_147-1

Introduction

Astronomy often involves studying objects so distant that they remain unresolved point sources with even the largest telescopes. Exoplanets are particularly difficult to study because they are small compared to other astronomical objects. Short of building a large interferometer to spatially resolve the disks of exoplanets, we must rely on chance and astronomical trickery to map the atmospheres and surfaces of exoplanets. (The diffraction limit dictates that resolving the disk of an Earth-sized planet at 10 pc requires a telescope – or array of telescopes – at least 24 km across at optical wavelengths or 600 km across in the thermal infrared.)

We expect planets to have spatial inhomogeneities for a few reasons: left to their own devices, atmospheres are subject to instabilities that produce spatially inhomogeneous temperature structure and time-variable clouds. Moreover, planets orbiting near a star are further subject to asymmetric radiative forcing from their star, leading to diurnal (day–night) and seasonal (summer–winter) variations. Lastly, the surface of a planet may have a heterogeneous character due to geological activity.

Although part of the motivation to map exoplanets is simply to know what they look like, there are undoubtedly cases where understanding a planet requires understanding the diversity of its different regions. We would therefore like to map the atmospheres and surfaces of exoplanets.

Mapping Basics

If we can detect light from an exoplanet, then we can try to map it, whether the planetary light is temporally separated (Charbonneau and Deming 2007), spatially separated (Marois et al. 2008), or spectrally separated (Snellen et al. 2010).

It is possible to map the surface of an unresolved object as long as we don't always see the same parts of it – the resulting changes in brightness can be detected across astronomical distances. We are therefore able to tease out spatial information about a planet based on its time-variable brightness, provided we know something about the viewing geometry. For distant astronomical objects, e.g., exoplanets, there are three ways in which our view changes: rotation of the planet, changes in its position with respect to its star, and occultations by another object (Fig. 1).

Rotational mapping is possible because at any given time, we only see light from at most a hemisphere and as the planet spins on its own axis, different atmospheric and surface features rotate in and out of view. Orbital mapping with reflected light is possible due to the changing illumination pattern as the planet orbits its star. Occultation mapping, on the other hand, requires a second object to pass in front of the planet – the host star is the most likely culprit. The occulting object progressively obscures the planet, hence changing our view and the system's overall flux. (It is also possible to distinguish the western and eastern terminators of a transiting planet by comparing ingress and egress transmission spectra: scale height (Dobbs-Dixon et al. 2012), winds (Louden and Wheatley 2015), or aerosols (Kempton and Bean 2017) – we do not discuss these methods since they do not involve planetary light.) In

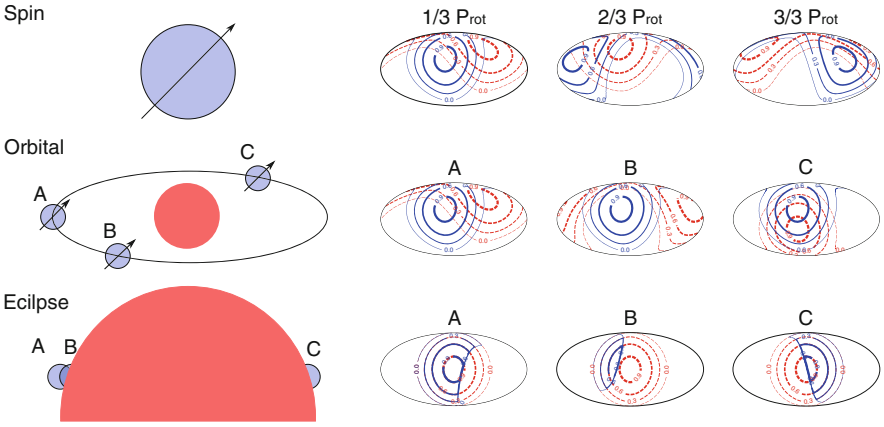

Fig. 1 The visibility (*blue contours*) and illumination (*red contours*) at three times for the different exoplanet mapping techniques: rotational mapping (*top*), orbital mapping (*middle*), and eclipse mapping (*bottom*). For the *top two panels*, we adopt an inclination of 60° and the planetary obliquity is 45°. For thermal emission, the convolution kernel is proportional to the visibility, while for diffuse reflected light the kernel is proportional to the product of visibility and illumination (see the Kernel section below). When the planet is unocculted (*top two rows*), the nonzero regions of the visibility and illumination are each hemispheres, making the nonzero portion of the reflection kernel a lune. For the occultation geometry shown in the *bottom row*, we've assumed that the planet is slowly rotating so that essentially the same hemisphere is facing the observer before and after the occultation

practice, multiple sources of variability can be present in a single data set: phase variations are generally accompanied by rotation of the planet, and occultations are usually accompanied by some phase variations.

Mapping Formalism

Exo-cartography is an *inverse problem*, as opposed to the *forward problem* of predicting the reflected or emitted spectrum of a planet based on its surface and atmospheric properties. The usual approach to the inverse problem is to solve the forward problem many times with varying map parameters to see which one best approximates the disk-integrated observations.

State-of-the-art forward modeling involves, at the very least, detailed radiative transfer calculations and hence is not useful for solving the inverse problem (Robinson et al. 2011). One of the necessities of tackling the inverse problem is therefore making judicious simplifications. Adopting the notation of Cowan et al. (2013), the forward problem is approximated as linear:

$$F(t) = \oint K(\theta, \phi, t) M(\theta, \phi) d\Omega, \tag{1}$$

where $F(t)$ is the observed flux, or light curve, $K(\theta, \phi, t)$ is the kernel, $M(\theta, \phi)$ is the top-of-atmosphere planet map, θ and ϕ are planetary colatitude and longitude, respectively, the differential solid angle is $d\Omega = \sin\theta d\theta d\phi$ for a spherical planet, and $\oint d\Omega$ is the integral over the entire planet. Although F stands for "flux," the units of $F(t)$ depend on the situation and chosen normalization: planetary flux, planet/star flux ratio, reflectance, apparent albedo, etc.

Arguably the most important simplification we have made is assuming a static map, $\partial M/\partial t = 0$, as it is generally intractable to map the surface of an unresolved planet when that map is changing. One can succeed, however, if the planet varies more slowly than our view of it. For example, large-scale cloud patterns on Earth evolve slowly compared to the planet's rotation (Cowan et al. 2009), and some eccentric planets may still be amenable to eclipse mapping, despite seasonal variations in temperature and cloud cover. Beyond these exceptions, one must adopt a parameterized time-variable map, $M(\theta, \phi, t)$. This approach allowed Lewis et al. (2013) to use the energy balance model of Cowan and Agol (2011) to fit infrared phase curves of an eccentric hot Jupiter. Finally, Cowan et al. (2017) showed that in special circumstances – namely, planets on circular, edge-on orbits – one can infer a time-variable map based on the presence of certain modes; nonetheless, this is a far cry from mapping the changing surface of a planet.

If the map is static, then time variations only come in through the kernel. If there are no occultations, then the changing sub-observer and substellar locations dictate the time variability of the kernel and hence the time variations in observed flux (for thermal emission, only the sub-observer location is relevant). Schwartz et al. (2016) therefore derived closed-form analytic expressions for the sub-observer and substellar colatitude and colongitude for planets on circular orbits.

The Inverse Problem

Inverse problems are typically under-constrained, and exo-cartography is no exception. First of all, there may be nonzero maps that produce flat light curves, a so-called nullspace. Secondly, different maps sometimes produce identical light curves. These represent the loss of information: one can only recover a perfectly faithful map by spatially resolving the disk of the planet. The bottom line is that attempts to map the brightness markings of distant objects suffer from formal degeneracies, even in the limit of noiseless observations.

If the orientation of the planet is not known a priori, then the problem is even more challenging because the kernel is a function of one or more unknown parameters: spin frequency, spin orientation, etc. Nonetheless, it has been demonstrated in numerical experiments that one can extract a planet's spin (rotation rate, obliquity, and its direction) from reflected light curves (Pallé et al. 2008; Oakley and Cash 2009; Kawahara and Fujii 2010, 2011; Fujii and Kawahara 2012; Schwartz et al. 2016; Kawahara 2016) or from thermal light curves (Gaidos and Williams 2004; de Kok et al. 2011; Gómez-Leal et al. 2012; Cowan et al. 2012c, 2013).

Exoplanets can be mapped using single-band photometry to produce a monochrome map or using spectrally resolved data to produce maps at each wavelength. It is often more insightful, however, to assume that the light curves are correlated due to common viewing geometry, molecular absorption, or surface spectra. The inverse problem of mapping a planet using template spectra – let alone retrieving intrinsic surface colors and spectra – based on multiband data is beyond the scope of this review but has been considered in the literature (Cowan et al. 2009, 2011; Fujii et al. 2010, 2011, 2017; Kostov and Apai 2013; Cowan and Strait 2013; Buenzli et al. 2014; Stevenson et al. 2014).

The Kernel

The kernel is the equivalent to the vertical contribution function in 1D atmospheric radiative transfer (Kawahara and Fujii use "weight" to refer to the kernel). By definition, the kernel must move over the planet in order for exo-cartography to be possible. The shape of the kernel, however, is constant for rotational mapping and thermal phase mapping. For such a static kernel, some maps are always in the nullspace, leading to severe degeneracy in the inverse problem. If the shape of the kernel changes with time, then maps need not remain in the nullspace; this is the case for eclipse mapping or reflected-light mapping involving both rotation and orbital motion. The degeneracy-busting power of a changing kernel is analogous to how a changing antenna pattern dramatically reduces the degeneracy in the location of a radio source on the sky.

Thermal Emission

For thermal emission problems, the kernel is simply the normalized visibility:

$$K(\theta, \phi, t) = \frac{1}{\pi} V(\theta, \phi, t), \tag{2}$$

where the visibility, V, is unity at the sub-observer location (the center of the planetary disk as seen by the observer), drops as the cosine of the angle from the sub-observer location, and is zero on the far side of the planet or any part of the planet hidden from view by another object (e.g., an occulting star or moon). Cowan et al. (2013) derived analytic light curves for spherical harmonic basis maps in the absence of occultations. Due to the unchanging kernel shape, a large fraction of spherical harmonics are in the nullspace, limiting the accuracy of retrieved maps.

Reflected Light

For diffuse reflected light (a.k.a. Lambertian reflection), the kernel is the product of visibility and illumination:

$$K(\theta, \phi, t) = \frac{1}{\pi} V(\theta, \phi, t) I(\theta, \phi, t), \tag{3}$$

where the visibility is defined as above, and the illumination is unity at the substellar location (the center of the planetary disk as seen from the star), drops as the cosine of the angle from the substellar location, and is zero on the night side of the planet or any part of the planet in the shadow of another object (e.g., an eclipsing planet or moon). Analytic reflected light curves have so far been derived for spherical harmonics in only a few special cases, namely, at opposition phase (Russell 1906), and for tidally locked, edge-on geometry (Cowan et al. 2013). Extending this framework to polarized reflected light is beyond the scope of this review but would undoubtedly yield useful constraints on cloud and surface properties (e.g., Wiktorowicz and Stam 2015).

In practice, the Lambertian kernel is a suitable approximation for most planets at gibbous phases. But backscattering can be important at full phase, while forward scattering is important at crescent phases (Robinson et al. 2010). If glint is the dominant form of reflection on a planet, then the kernel is approximately a δ-function at the location of the glint spot (see Appendix C of Cowan et al. 2009): the light curve in this limit is a Boolean record of whether the glint spot is over cloud-free water or not. Even when it is not dominant, specular reflection from surface liquid water is important as it is a direct indication of habitability (Robinson et al. 2014, and see chapter, ▸ "Detecting Habitability").

Due to the combined effects of glint and forward scattering, one has to be wary when combining data from multiple orbital phases to construct a reflected light map of a planet. Nonetheless, simulations show that this can be done at quarter and gibbous phases (Fujii and Kawahara 2012).

Occultations

If a planet passes directly behind its star [see chapter ▸ "Characterization of Exoplanets: Secondary Eclipses"], then one may map its dayside. Eclipse mapping can be applied to either planetary emission or reflected light, but the contrast ratio makes the latter daunting.

While the eclipse depth is proportional to the integrated dayside brightness of the planet, the detailed shape of ingress and egress is a function of the spatial distribution of flux on the planet's dayside (Fig. 2). Although eclipses of planets by their host star have so far garnered the most attention, occultations by moons or other planets are also possible, especially in packed planetary systems like TRAPPIST-1 (Veras and Breedt 2017).

The kernel is discontinuous during occultations, making it more challenging to analytically solve the forward problem. To our knowledge, such solutions have not yet been developed, but by analogy with the related problem of a planet transiting a nonuniform star (Mandel and Agol 2002), we suspect that they exist.

Basis Maps and Basis Light Curves

The exo-cartography inverse problem boils down to fitting observed light curves. There are two parameterizations of the problem: one can use orthonormal basis maps (e.g., spherical harmonics)

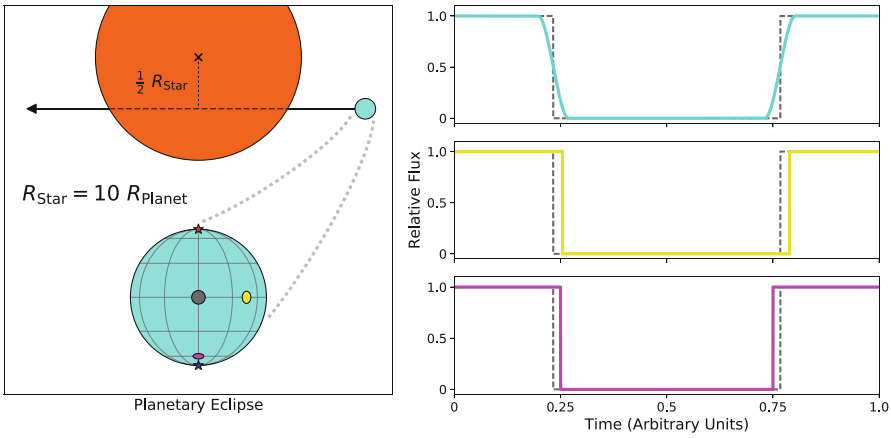

Fig. 2 Schematic showing the dominant signals present in secondary eclipse light curves. The *teal light curve* denotes a uniform planet (the "occultuniform" of Mandel and Agol 2002). The *gray dashed line* is the *eclipse shape* if the planetary flux is concentrated in the center of the disk (a caricature of limb darkening or the dayside hotspot of a short-period planet; Rauscher et al. 2007). The *yellow* and *magenta lines* show the light curves for the same concentrated bright spot at different locations on the planetary disk. In particular, the *yellow line* shows the effect of a longitudinal offset predicted by Williams et al. (2006) and measured by Agol et al. (2010). The *magenta line* shows the effect of a latitudinal offset predicted by Rauscher et al. (2007) and measured by Majeau et al. (2012) and de Wit et al. (2012). All of these signals suffer degeneracies with system geometry, notably impact parameter, planet/star radius ratio, and orbital eccentricity (de Wit et al. 2012). Fortunately, many of these degeneracies can be broken with spectrally resolved data (Dobbs-Dixon et al. 2015): the planetary map may be wavelength-dependent, but the system geometry cannot (Figure from J.C. Schwartz, private communication)

$$\frac{1}{4\pi}\oint M_1(\theta,\phi)M_2(\theta,\phi)d\Omega = \delta_{12}, \tag{4}$$

and repeatedly solve the forward problem in order to fit an observed light curve, or one can use orthonormal basis light curves (e.g., a Fourier series)

$$\frac{1}{P}\int_0^P L_1(t)L_2(t)dt = \delta_{12}, \tag{5}$$

to directly fit the observed light curve and then identify the associated map and its uncertainties in post-processing. Sometimes, orthonormal basis maps produce orthonormal basis light curves, and the problem is particularly tidy. This is the case for rotational thermal mapping (Cowan and Agol 2008; Cowan et al. 2013). Usually, however, the adopted basis maps do not produce orthogonal light curves.

There are two broad classes of map parameterizations: global (e.g., spherical harmonics) and local (e.g., pixels). Examples of both basis maps are shown in Fig. 3. The optimal basis maps will depend on viewing geometry, expected map geometry, and the nature of the data. In general, spherical harmonics are better for rotational

mapping, smoothly varying maps, and/or full phase coverage. Pixels are preferable for eclipse mapping, sharp features, and/or partial phase coverage.

A related consideration is the nullspace for a given convolution: it is usually best to use basis maps for which some maps are well-constrained and others are unambiguously in the nullspace as this makes the degeneracies easier to track down. It is not always easy to guess which maps will be in the nullspace: counterintuitively, thermal rotational mapping and reflected phase variations of a zero-obliquity planet are nonetheless sensitive to the north–south asymmetry a planet's map (Cowan et al. 2012a, 2013, 2017).

As with many under-constrained inverse problems, it is often necessary to apply a prior on the model parameters, especially when the data are noisy. For exo-cartography, this takes the form of regularization to enforce smoothness between pixels (e.g., Knutson et al. 2007; Kawahara and Fujii 2010, 2011; Fujii and Kawahara 2012) and suppressing power in high-order modes (e.g., Cowan and Agol 2008; Majeau et al. 2012).

Pixels and Slices

An intuitive approach is to pixelize the planetary surface. The most general pixelization scheme is two-dimensional, for example, a lat–lon grid of pixels or HEALPix (http://healpix.sourceforge.net/). This is useful if the kernel moves or changes its shape in more than one direction, e.g., eclipse mapping or rotational reflected light curves at multiple orbital phases.

Denoting the intensity of the n-th pixel by m_n,

$$M(\theta,\phi) = \sum m_n M_n(\theta,\phi), \tag{6}$$

where the basis maps are

$$M_n(\theta,\phi) = \begin{cases} 1 & \text{if } \{\theta,\phi\} \in\ n-\text{th pixel}, \\ 0 & \text{otherwise.} \end{cases} \tag{7}$$

As a pixel gets smaller, it is well approximated by a δ-function at its center. Although δ-functions are terrible basis maps for decomposing real-life continuous maps, they have the advantage of being trivial to integrate:

$$F_{\theta\phi}(t) = \oint K(\theta',\phi',t)\delta(\theta'-\theta,\phi'-\phi)d\Omega' \tag{8}$$

$$= K(\theta,\phi,t). \tag{9}$$

For rotational mapping, latitudinal information is difficult to extract, so it is often reasonable to consider a map consisting of north–south uniform slices (like a beach ball). This situation includes rotational mapping of reflected light at a fixed orbital phase and rotational mapping of thermal infrared.

Spherical Harmonics

Any continuous albedo map, $M(\theta, \phi)$, may be decomposed into spherical harmonics:

$$M(\theta, \phi) = \sum_{l=0}^{\infty} \sum_{m=-l}^{l} C_l^m Y_l^m(\theta, \phi), \tag{10}$$

$$C_l^m = \frac{1}{4\pi} \oint M(\theta, \phi) Y_l^m(\theta, \phi) d\Omega. \tag{11}$$

In certain applications it is all but hopeless to glean latitudinal information (but see Cowan et al. 2013, 2017). Here it is expedient to adopt sinusoidal basis maps, essentially spherical harmonics, but setting $m = l$ (or, equivalently, integrating Y_l^m over latitude: Cowan and Agol 2008).

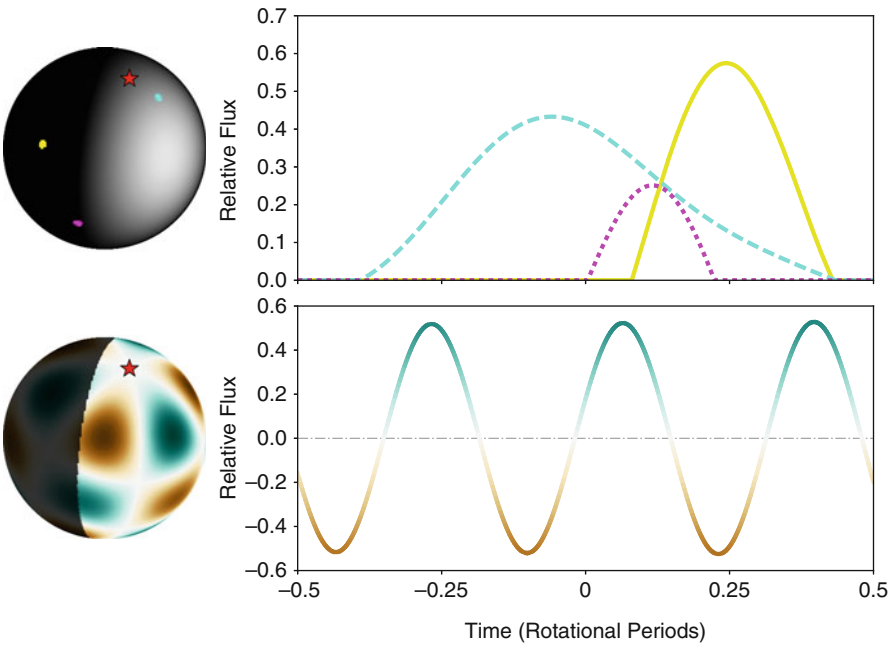

Fig. 3 Basis maps and their reflected light curves. Examples of δ-maps (*top*) and a spherical harmonic map (*bottom*). For the δ-functions of the *top panel*, the resulting light curves are simply the value of the kernel at a particular location on the planet as a function of time, making them trivial to compute; small pixels would have approximately the same light curves. For the spherical harmonic map in the *bottom panel*, note that the resulting light curve is conveniently sinusoidal. The *red star* in each image denotes the north planetary pole; the planet rotates to the east (Figure from J.C. Schwartz, private communication)

Current Results and Future Prospects

Spitzer Space Telescope phase curves have so far been reported for a handful of short-period planets on circular orbits (Eccentric planets undergo seasonal variations and hence are not amenable to phase mapping.): HD 189733b (Knutson et al. 2007, 2009b, 2012), HD 149026b (Knutson et al. 2009a), WASP-12b (Cowan et al. 2012b), WASP-18b (Maxted et al. 2013), HD 209458b (Zellem et al. 2014), WASP-14b (Wong et al. 2015), WASP-19b and HAT-P-7b (Wong et al. 2016), and 55 Cancri-e (Demory et al. 2016), and WASP-43b (Stevenson et al. 2017). In some cases these phase curves have been converted to longitudinal brightness maps (e.g., using Eqn 7 of Cowan and Agol 2008), while in others the mapping was left to the imagination and may not be physically plausible (Keating & Cowan 2016).

Eclipse mapping has so far been performed on HD 189733b with 8 micron measurements from *Spitzer* (Majeau et al. 2012; de Wit et al. 2012). Figure 4 shows the combined phase+eclipse map of HD 189733b from Majeau et al. (2012) showing both longitudinal and latitudinal information, making this a coarse 2D map.

Demory et al. (2013) constructed an albedo map of the hot Jupiter Kepler-7b based on phase curves from the Kepler mission (Fig. 5). Also using Kepler photometry, Armstrong et al. (2016) made maps of the changing atmosphere of the hot Jupiter HAT-P-7b. Many other researchers have analyzed *Kepler* phase curves to understand the albedo and temperature maps of short-period giant planets without explicitly constructing longitudinal brightness maps (e.g., Esteves et al. 2013, 2015; Shporer et al. 2014; Angerhausen et al. 2015).

Stevenson et al. (2014) analyzed Hubble Space Telescope WFC3 spectral phase curves of WASP-43b. Since the wavelengths probed spanned a water absorption

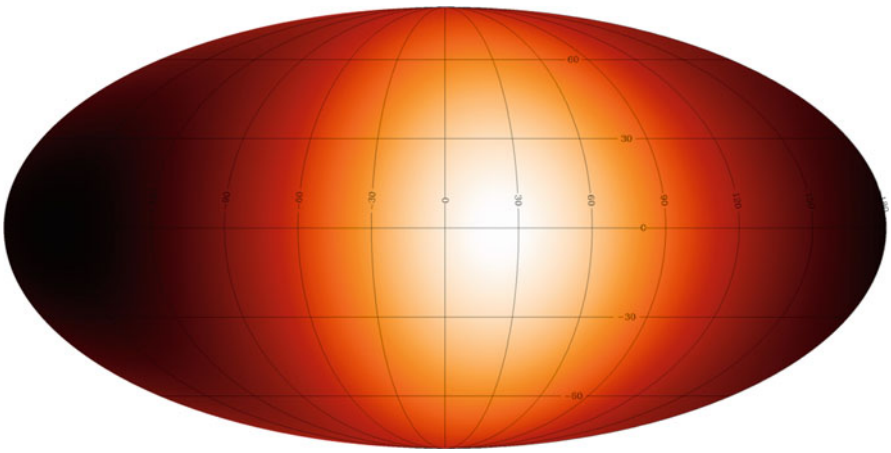

Fig. 4 Two-dimensional thermal map of the hot Jupiter HD 189733b, based on mid-infrared phase and eclipse measurements from the Spitzer Space Telescope (From Majeau et al. 2012). The substellar point is in the center of the map. The equatorial hotspot indicates a small obliquity, while the eastward offset is probably due to super-rotating zonal winds

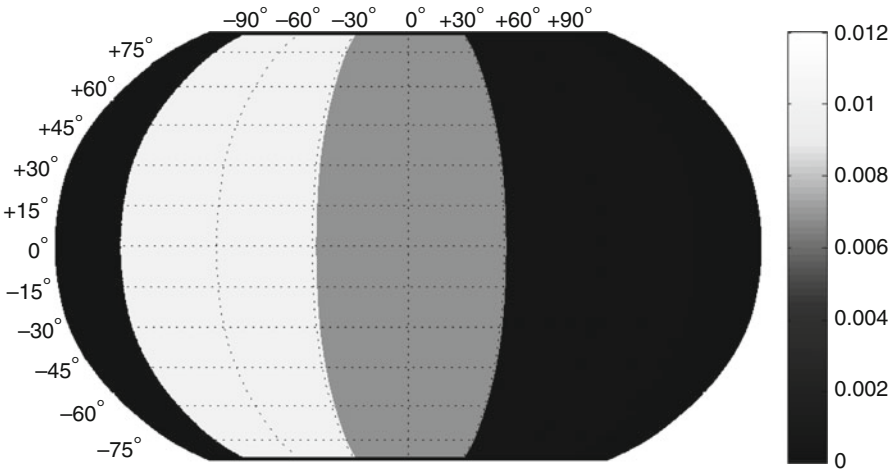

Fig. 5 Map of normalized intensity, I_p/I_*, for the planet Kepler-7b based on orbital phase variations measured by the Kepler mission (Adapted from Demory et al. 2013). If the planetary light is interpreted as reflected light, then the albedo is proportional to intensity, $A_g = (I_p/I_*)(a/R_*)^2$, and the bright region on the planet's western hemisphere has an albedo of 0.64, suggestive of reflective clouds (e.g., Sudarsky et al. 2000). One possible explanation for the curious cloud pattern is that particles condense on the planet's cooler nightside, are advected to the dayside by eastward winds, and sublimate when the star is overhead (e.g., Heng and Demory 2013; Parmentier et al. 2016)

band and hence different heights in the atmosphere, they were able to construct a 2D temperature map of the planet (longitude and altitude). [See chapter ▸ "Characterization of Exoplanets: Observations and Modeling of Orbital Phase Curves" for a review of phase curves, both thermal and reflected.]

In the near future, the James Webb Space Telescope will provide qualitatively better observations of short-period planets (Beichman et al. 2014; Cowan et al. 2015). In principle, wavelength-dependent eclipse and phase measurements should enable 3D temperature maps of the daysides of hot Jupiters and 2D (longitude and altitude) temperature maps of their nightsides. The spectral resolution and wavelength coverage of JWST will also allow us to distinguish between thermal emission and reflected light (Schwartz and Cowan 2015; Parmentier et al. 2016; Keating & Cowan 2016), as well as disentangling phase variations, star spots, Doppler beaming, and ellipsoidal variations (Cowan et al. 2012b; Knutson et al. 2012; Esteves et al. 2015).

Current direct imaging experiments like GPI and SPHERE have detected the rotation of an exoplanet via rotational Doppler broadening (Snellen et al. 2014) and in principle could detect variations in thermal emission from planets due to rotation of patchy clouds in and out of view, as is currently performed for brown dwarfs [see chapter, ▸ "Variability of Brown Dwarfs"]. The next generation of ground-based telescopes should enable both photometric mapping and Doppler tomography of giant planets (Crossfield et al. 2014).

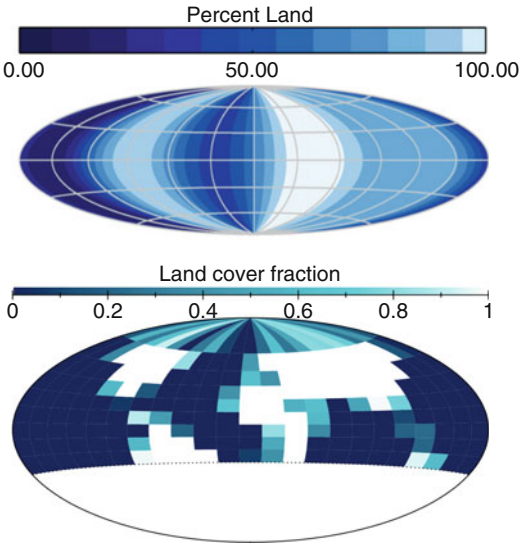

Fig. 6 *Top*: A one-dimensional color map of Earth based on 24 h of disk-integrated photometry obtained by the Deep Impact spacecraft as part of the EPOXI mission (From Cowan et al. 2009). *Bottom*: A two-dimensional surface map recovered from simulated full-orbit multiband observations of a cloud-free Earth twin (From Kawahara and Fujii 2011); in this simulation the observer was at northern latitudes and hence could not map the southern portion of the planet. One can readily identify the major landforms and oceans in either of these maps, unambiguously identifying this planet as habitable

NASA's WFIRST mission will directly image Jupiter analogs in reflected light, hence enabling rotational mapping of their clouds. Future space-based direct imaging missions like LUVOIR and HabEx will enable reflected light surface mapping and spin determination for terrestrial planets (Pallé et al. 2008; Oakley and Cash 2009; Cowan et al. 2009, 2011; Kawahara and Fujii 2010, 2011; Fujii and Kawahara 2012; Cowan and Strait 2013; Fujii et al. 2017, Fig. 6). The bimodal surface character of Earth may be crucial to its long-term habitability, so constructing surface maps of terrestrial exoplanets will be a step toward understanding habitable environments outside of the solar system (Abbot et al. 2012; Cowan and Abbot 2014; Foley 2015; Cowan 2015; Komacek and Abbot 2016).

Clouds are a blessing and a curse to exo-cartography and are likely to present a challenge for the foreseeable future. From Earth to brown dwarfs, clouds contribute to the spatial inhomogeneity that make exo-cartography interesting and feasible. But clouds also mask underlying features and often vary in time. We therefore expect that much of the future effort in exo-cartography will be dedicated to mapping clouds and devising schemes to minimize their effects in order to catch glimpses of the planetary surface below.

Cross-References

- ▸ Characterization of Exoplanets: Observations and Modeling of Orbital Phase Curves
- ▸ Characterization of Exoplanets: Secondary Eclipses
- ▸ Detecting Habitability
- ▸ Variability of Brown Dwarfs

Acknowledgements The authors are grateful to International Space Science Institute for hosting the Exo-Cartography workshops. N.B. Cowan acknowledges support from the McGill Space Institute and l'Institut de recherche sur les exoplanètes. Y. Fujii was supported by the NASA Postdoctoral Program at the NASA Goddard Institute for Space Studies, administered by Universities Space Research Association, as well as by the NASA Astrobiology Program through the Nexus for Exoplanet System Science. The authors thank J.C. Schwartz for creating many of the figures, as well as T. Bell, D. Keating, E. Rauscher, and T. Robinson for providing useful feedback on an earlier draft of this review.

References

Abbot DS, Cowan NB, Ciesla FJ (2012) Indication of insensitivity of planetary weathering behavior and habitable zone to surface land fraction. ApJ 756:178

Agol E, Cowan NB, Knutson HA et al (2010) The climate of HD 189733b from fourteen transits and eclipses measured by Spitzer. ApJ 721:1861–1877

Angerhausen D, DeLarme E, Morse JA (2015) A comprehensive study of Kepler phase curves and secondary eclipses: temperatures and albedos of confirmed Kepler giant planets. PASP 127:1113

Armstrong DJ, de Mooij E, Barstow J et al (2016) Variability in the atmosphere of the hot giant planet HAT-P-7 b. Nat Astron 1:0004

Beichman C, Benneke B, Knutson H et al (2014) Observations of transiting exoplanets with the James Webb Space Telescope (JWST). PASP 126:1134

Buenzli E, Apai D, Radigan J, Reid IN, Flateau D (2014) Brown dwarf photospheres are patchy: a hubble space telescope near-infrared spectroscopic survey finds frequent low-level variability. ApJ 782:77

Charbonneau D, Deming D (2007) The dynamics-based approach to studying terrestrial exoplanets. arXiv:0706.1047

Cowan NB (2015) Water on -and in- terrestrial planets. arXiv:1511.04444

Cowan NB, Abbot DS (2014) Water cycling between ocean and mantle: super-Earths need not be waterworlds. ApJ 781:27

Cowan NB, Agol E (2008) Inverting phase functions to map exoplanets. ApJ 678:L129–L132

Cowan NB, Agol E (2011) A model for thermal phase variations of circular and eccentric exoplanets. ApJ 726:82

Cowan NB, Strait TE (2013) Determining reflectance spectra of surfaces and clouds on exoplanets. ApJ 765:L17

Cowan NB, Agol E, Meadows VS et al (2009) Alien maps of an ocean-bearing world. ApJ 700:915–923

Cowan NB, Robinson T, Livengood TA et al (2011) Rotational variability of Earth's polar regions: implications for detecting snowball planets. ApJ 731:76

Cowan NB, Abbot DS, Voigt A (2012a) A false positive for ocean glint on exoplanets: the latitude-Albedo effect. ApJ 752:L3
Cowan NB, Machalek P, Croll B et al (2012b) Thermal phase variations of WASP-12b: defying predictions. ApJ 747:82
Cowan NB, Voigt A, Abbot DS (2012c) Thermal phases of Earth-like planets: estimating thermal inertia from eccentricity, obliquity, and diurnal forcing. ApJ 757:80
Cowan NB, Fuentes PA, Haggard HM (2013) Light curves of stars and exoplanets: estimating inclination, obliquity and albedo. MNRAS 434:2465–2479
Cowan NB, Greene T, Angerhausen D et al (2015) Characterizing transiting planet atmospheres through 2025. PASP 127:311
Cowan NB, Chayes V, Bouffard É, Meynig M, Haggard HM (2017) Odd harmonics in exoplanet photometry: weather or artifact? MNRAS 467:747–757
Crossfield IJM, Biller B, Schlieder JE et al (2014) A global cloud map of the nearest known brown dwarf. Nature 505:654–656
de Kok RJ, Stam DM, Karalidi T (2011) Characterizing exoplanetary atmospheres through infrared polarimetry. ApJ 741:59
de Wit J, Gillon M, Demory BO, Seager S (2012) Towards consistent mapping of distant worlds: secondary-eclipse scanning of the exoplanet HD 189733b. A&A 548:A128
Demory BO, de Wit J, Lewis N et al (2013) Inference of inhomogeneous clouds in an exoplanet atmosphere. ApJ 776:L25
Demory BO, Gillon M, de Wit J et al (2016) A map of the large day-night temperature gradient of a super-Earth exoplanet. Nature 532:207–209
Dobbs-Dixon I, Agol E, Burrows A (2012) The impact of circumplantary jets on transit spectra and timing offsets for hot Jupiters. ApJ 751:87
Dobbs-Dixon I, Agol E, Deming D (2015) Spectral eclipse timing. ApJ 815:60
Esteves LJ, De Mooij EJW, Jayawardhana R (2013) Optical phase curves of Kepler exoplanets. ApJ 772:51
Esteves LJ, De Mooij EJW, Jayawardhana R (2015) Changing phases of alien worlds: probing atmospheres of Kepler planets with high-precision photometry. ApJ 804:150
Foley BJ (2015) The role of plate tectonic-climate coupling and exposed land area in the development of habitable climates on rocky planets. ApJ 812:36
Fujii Y, Kawahara H (2012) Mapping Earth analogs from photometric variability: spin-orbit tomography for planets in inclined orbits. ApJ 755:101
Fujii Y, Kawahara H, Suto Y et al (2010) Colors of a second Earth: estimating the fractional areas of ocean, land, and vegetation of Earth-like exoplanets. ApJ 715:866–880
Fujii Y, Kawahara H, Suto Y et al (2011) Colors of a second Earth. II. Effects of clouds on photometric characterization of Earth-like exoplanets. ApJ 738:184
Fujii, Y., Lustig-Yaeger, J., & Cowan, N. B. 2017, arXiv:1708.04886
Gaidos E, Williams DM (2004) Seasonality on terrestrial extrasolar planets: inferring obliquity and surface conditions from infrared light curves. New Astron 10:67–77
Gómez-Leal I, Pallé E, Selsis F (2012) Photometric variability of the disk-integrated thermal emission of the Earth. ApJ 752:28
Heng K, Demory BO (2013) Understanding trends associated with clouds in irradiated exoplanets. ApJ 777:100
Kawahara H (2016) Frequency modulation of directly imaged exoplanets: geometric effect as a probe of planetary obliquity. ApJ 822:112
Kawahara H, Fujii Y (2010) Global mapping of Earth-like exoplanets from scattered light curves. ApJ 720:1333–1350
Kawahara H, Fujii Y (2011) Mapping clouds and terrain of Earth-like planets from photometric variability: demonstration with planets in face-on orbits. ApJ 739:L62
Keating, D., & Cowan, N. B. 2016, arXiv:1709.03502
Kempton EMR, Bean JL, Parmentier V (2017) An observational diagnostic for distinguishing between clouds and haze in hot exoplanet atmospheres. Astrophys J Lett 845:L20

Knutson HA, Charbonneau D, Allen LE et al (2007) A map of the day-night contrast of the extrasolar planet HD 189733b. Nature 447:183–186
Knutson HA, Charbonneau D, Burrows A, O'Donovan FT, Mandushev G (2009a) Detection of a temperature inversion in the broadband infrared emission spectrum of TrES-4. ApJ 691: 866–874
Knutson HA, Charbonneau D, Cowan NB et al (2009b) Multiwavelength constraints on the day-night circulation patterns of HD 189733b. ApJ 690:822–836
Knutson HA, Lewis N, Fortney JJ et al (2012) 3.6 and 4.5 μm phase curves and evidence for non-equilibrium chemistry in the atmosphere of extrasolar planet HD 189733b. ApJ 754:22
Komacek TD, Abbot DS (2016) Effect of surface-mantle water exchange parameterizations on exoplanet ocean depths. ApJ 832:54
Kostov V, Apai D (2013) Mapping directly imaged giant exoplanets. ApJ 762:47
Lewis NK, Knutson HA, Showman AP et al (2013) Orbital phase variations of the eccentric giant planet HAT-P-2b. ApJ 766:95
Louden T, Wheatley PJ (2015) Spatially resolved eastward winds and rotation of HD 189733b. ApJ 814:L24
Majeau C, Agol E, Cowan NB (2012) A Two-dimensional infrared map of the extrasolar planet HD 189733b. ApJ 747:L20
Mandel K, Agol E (2002) Analytic light curves for planetary transit searches. ApJ 580:L171–L175
Marois C, Macintosh B, Barman T et al (2008) Direct imaging of multiple planets orbiting the star HR 8799. Science 322:1348
Maxted PFL, Anderson DR, Doyle AP et al (2013) Spitzer 3.6 and 4.5 μm full-orbit light curves of WASP-18. MNRAS 428:2645–2660
Oakley PHH, Cash W (2009) Construction of an Earth model: analysis of exoplanet light curves and mapping the next Earth with the new worlds observer. ApJ 700:1428–1439
Pallé E, Ford EB, Seager S, Montañés-Rodríguez P, Vazquez M (2008) Identifying the rotation rate and the presence of dynamic weather on extrasolar Earth-like planets from photometric observations. ApJ 676:1319–1329
Parmentier V, Fortney JJ, Showman AP, Morley C, Marley MS (2016) Transitions in the cloud composition of hot Jupiters. ApJ 828:22
Rauscher E, Menou K, Seager S et al (2007) Toward eclipse mapping of hot Jupiters. ApJ 664:1199–1209
Robinson TD, Meadows VS, Crisp D (2010) Detecting oceans on extrasolar planets using the glint effect. ApJ 721:L67–L71
Robinson TD, Meadows VS, Crisp D et al (2011) Earth as an extrasolar planet: earth model validation using EPOXI Earth observations. Astrobiology 11:393–408
Robinson TD, Ennico K, Meadows VS et al (2014) Detection of ocean glint and ozone absorption using LCROSS Earth observations. ApJ 787:171
Russell HN (1906) On the light variations of asteroids and satellites. ApJ 24:1–18
Schwartz JC, Cowan NB (2015) Balancing the energy budget of short-period giant planets: evidence for reflective clouds and optical absorbers. MNRAS 449:4192–4203
Schwartz JC, Sekowski C, Haggard HM, Pallé E, Cowan NB (2016) Inferring planetary obliquity using rotational and orbital photometry. MNRAS 457:926–938
Shporer A, O'Rourke JG, Knutson HA et al (2014) Atmospheric characterization of the hot Jupiter Kepler-13Ab. ApJ 788:92
Snellen IAG, de Kok RJ, de Mooij EJW, Albrecht S (2010) The orbital motion, absolute mass and high-altitude winds of exoplanet HD209458b. Nature 465:1049–1051
Snellen IAG, Brandl BR, de Kok RJ et al (2014) Fast spin of the young extrasolar planet β Pictoris b. Nature 509:63–65
Stevenson KB, Désert JM, Line MR et al (2014) Thermal structure of an exoplanet atmosphere from phase-resolved emission spectroscopy. Science 346:838–841
Sudarsky D, Burrows A, Pinto P (2000) Albedo and reflection spectra of extrasolar giant planets. ApJ 538:885–903

Veras D, Breedt E (2017) Eclipse, transit and occultation geometry of planetary systems at exo-syzygy. MNRAS 468:2672–2683

Wiktorowicz SJ, Stam DM (2015) Polarimetry of Stars and Planetary Systems, Edited by L. Kolokolova, J. Hough, and A. Levasseur-Regourd. ISBN: 978-1-107-04390-9. Cambridge University Press, 2015, p.439

Williams PKG, Charbonneau D, Cooper CS, Showman AP, Fortney JJ (2006) Resolving the surfaces of extrasolar planets with secondary eclipse light curves. ApJ 649:1020–1027

Wong I, Knutson HA, Lewis NK et al (2015) 3.6 and 4.5 μm phase curves of the highly irradiated eccentric hot Jupiter WASP-14b. ApJ 811:122

Wong I, Knutson HA, Kataria T et al (2016) 3.6 and 4.5 μm Spitzer phase curves of the highly irradiated hot Jupiters WASP-19b and HAT-P-7b. ApJ 823:122

Zellem RT, Lewis NK, Knutson HA et al (2014) The 4.5 μm full-orbit phase curve of the hot Jupiter HD 209458b. ApJ 790:53